5 May 2000

ELSEVIER

Chemical Physics Letters 321 (2000) 363–371

CHEMICAL PHYSICS LETTERS

www.elsevier.nl/locate/cplett

# Exact computation of the triply periodic G ('Gyroid') minimal surface

Paul J.F. Gandy, Jacek Klinowski *

*Department of Chemistry, University of Cambridge, Lensfield Road, Cambridge, CB2 1EW, UK*

Received 7 March 2000; in final form 21 March 2000; accepted 21 March 2000

**Abstract**

Parametrization of the G triply periodic minimal surface, found in many physical, chemical and biological systems, has allowed us to calculate its coordinates analytically, and fully to describe its properties, such as the surface-to-volume ratio. Real structures may now be quantitatively compared with the precise coordinates and quantified in terms of the surface parameters. © 2000 Elsevier Science B.V. All rights reserved.

## 1. Introduction

A minimal surface is a surface which has a minimum area with zero mean curvature $H = (k_1 + k_2)/2$ at every point, where $k_1$ and $k_2$ are the principal curvatures [1]. A triply periodic minimal surface (TPMS) is a minimal surface which is periodic in three independent directions. When it is free of self-intersections it is said to be embedded. TPMS are described in terms of a fundamental patch ('Flächenstück') or asymmetric unit from which the entire surface may be built up by its symmetry elements.

Omnipresent in the natural and man-made worlds, TPMS provide concise, unified descriptions of seemingly unrelated structures [2], and are of interest not only to the structural chemist, but also in biology and morphogenesis [3], structural engineering and the science of materials [4], and are echoed in art and architecture [5]. Structural features of the G surface (also known as the gyroid) [6] have been found by X-ray diffraction in bicontinuous cubic systems in AB diblock copolymers [7], in lecithin–water and lipid–water systems [8], and in many other systems at high surfactant concentrations. The G surface separates the two networks postulated for the structure of strontium myristate [8], and is also found in $Ta_6Cl_{15}$ [9]. The gyroid phase is usually found in phase diagrams between the hexagonal and lamellar mesophases. The topological analogue of the G surface is the Y** periodic zero equipotential surface [10] found in compounds with the $Ca_3[Al_2Si_3O_{12}]$ garnet structure, which have applications in optoelectronic colour displays and the memory of magnetic bubbles in epitaxial garnet films [11]. Cell mem-

* Corresponding author. Fax: +44-1223-336362; e-mail: jk18@cam.ac.uk


PII: S0009-2614(00)00373-0

branes in living organisms such as the endoplasmic reticulum (where cell proteins and lipids are synthesised) are known to have a complex three-dimensional morphology, which corresponds to TPMS [12].

The fundamental structures identified in cellular organella are the cubic G, D and P surfaces. The partition of space by the surface in the organella enables cells to control the concentrations of various molecules and their transport across the bilayers. The surfactant can be used as a template for polymerisation reactions where the final product is the ordered mesoporous silica molecular sieve with well defined pore sizes and shapes [13], or hydrogels used as contact lenses [14]. Apart from the lamellar and hexagonal microstructures, the bicontinuous gyroid structure is formed. In the cetyltrimethylammonium chloride/$SiO_2$ system for high fraction of both components, the gyroid phase forms in which the single infinite silicate sheet separates the surfactant into two equal and disconnected sub-volumes. The mid plane of the silicate sheet in the inorganic mesoporous MCM-48 is the gyroid [15,16]. Although its structure is amorphous on the microscopic scale, the mid plane of the silica wall rests on the gyroid. The structure contains a three-dimensional channel network with channels running along {1, 1, 1} and {1, 0, 0} directions. The channel system in MCM-48 may be viewed as a collection of straight pores running in the four {1, 1, 1} directions related by the tetrahedral angle. The two channel systems form an enantiomorphic pair. Channel intersections reveal the spiral nature of both right- and left-handed pore systems with three channels spiralling around a central pore.

The fact that the G surface divides all space into two helical regions which are mirror images of one another is of special interest. Preparation of chiral catalysts and separation media which combine shape selectivity and enantioselectivity is a highly desirable objective in view of the increasing demand for enantiomerically pure compounds, especially for biological and pharmaceutical purposes [17]. Helical pores in inorganic materials might be able to act as such 'chiral filters', but their occurrence is rare [17] because helical structures (for example quartz) are commonly generated by a uni-directional symmetry element acting on an achiral structural subunit [18]. Amorphous silica gel, precipitated around chiral molecules (which are subsequently removed) may have such properties [19], but well-characterized crystalline materials would clearly be preferable for the purpose.

## 2. The Enneper–Weierstrass representation

TPMS are described in terms of the fundamental patch ('Flächenstück'): the smallest portion of the surface from which the entire surface can be constructed. The Enneper–Weierstrass representation [20] gives the coordinates of a minimal surface as

$$x = e^{i\theta}\mathrm{Re}\int_{\omega_o}^{\omega}(1-\tau^2)\,R(\tau)\,d\tau$$

$$y = e^{i\theta}\mathrm{Re}\int_{\omega_o}^{\omega} i(1+\tau^2)\,R(\tau)\,d\tau$$

$$z = e^{i\theta}\mathrm{Re}\int_{\omega_o}^{\omega} 2\tau R(\tau)\,d\tau \qquad (1)$$

where $i^2 = -1$ and $\tau = \tau_a + i\tau_b$, associating with function $R(\tau)$ (the Weierstrass function) a unique surface $r(\tau_a, \tau_b)$ which is guaranteed to be minimal; and $\theta$ is the so-called Bonnet angle. The Cartesian coordinates of any point are expressed as the real parts (Re) of contour integrals, evaluated in the complex plane from some fixed point $\omega_o$ to a variable point $\omega$. A specific minimal surface can be determined by integrating its Weierstrass function. The integrals (1) can always be evaluated by numerical integration, but so far could be calculated analytically for only a few surfaces [21–26].

Using the Bonnet transformation, fully described by the Bonnet angle, we can generate from a minimal surface a family of minimal surfaces with the same metric and Gaussian curvatures. By changing $\theta$ we obtain associate surfaces; when $\theta = \pi/2$, the associate surface is known as the conjugate surface. With respect to the D surface, the Bonnet angles are $\theta = 90°$ (for the P surface) and $\theta = \mathrm{ArcCot}[K'/K] = 38.0147°$, where $K = \mathrm{Elliptic}\,K[1/4]$ and $K' = \mathrm{Elliptic}\,K[3/4]$ (for the G surface) [6].

Although the properties of the TPMS follow uniquely from the Weierstrass function, $R(\tau)$ [23], the function is known only for several TPMS of simple topology. The Weierstrass function may be constructed if there exists a surface patch from which

the whole TPMS can be generated by reflection or rotation of the patch using appropriate symmetry elements [23]. This is the case for the D, G and P surfaces, for which the Weierstrass function is [27]

$$R(\tau) = \frac{1}{\sqrt{\tau^8 + \lambda\tau^4 + 1}} \qquad (2)$$

with $\lambda = -14$.

In general, the Weierstrass function is specified solely by values of $\tau$ which correspond to flat ('umbilical') points on the minimal surface where the Gaussian curvature is zero, in a form $\Pi_i(\tau - \tau_i)^\eta$, where $\eta$ determines the topology of the surface.

In 1970 Schoen identified the G surface as one of a further 17 examples of intersection-free TPMS, in addition to the five cases already known [6]. Its generating space group is $I4_132$ and the symmetry of the surface is $Ia\bar{3}d$ (No. 230), with 96 equivalent positions. Consequently, it is possible to divide the unit cell into 96 equivalent asymmetric volumes related by the symmetry elements of its space group. The surface embeds an inversion centre which interchanges the two sides of the surface and also the two labyrinth networks which it partitions. The labyrinths of the G surface are 3-connected and are enantiomorphic: one labyrinth is left-handed, the other, right-handed. The genus of the surface, a measure of its connectedness, is 3. The fundamental patch of the G surface is inscribed in a trirectangular tetrahedron, so called by Coxeter [28], because its face angles include three right angles (Fig. 1a). This is its kaleidoscopic cell or fundamental region for groups of reflections in $\mathscr{R}^3$, i.e. the convex polyhedron which provides plane boundaries enclosing a finite minimal surface patch which can be replicated by reflection to yield an infinite TPMS without self-intersections.

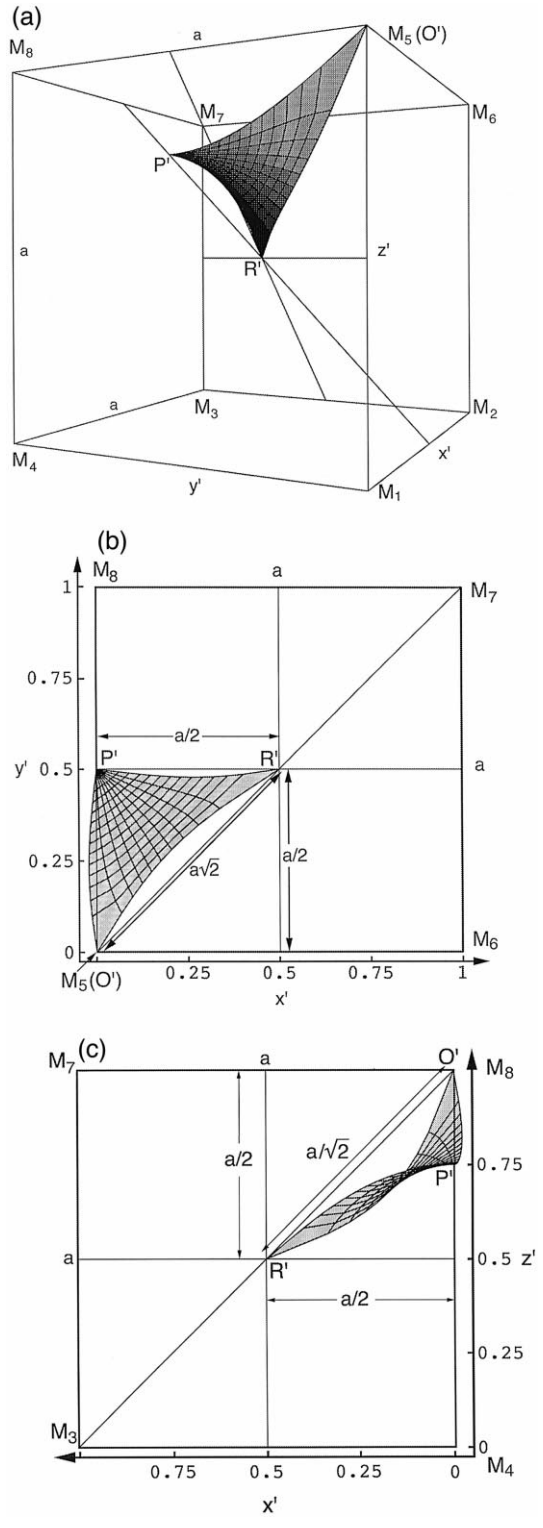


Fig. 1. (a) The fundamental patch of the G surface shown within its bounding cell (the cube with edge length $a$) is confined within two straight lines which pass through the origin and the adjacent diametrically opposed corners of the cube. The coordinate system has its origin at point $M_1$ and its orientation is indicated by the axes shown. Flat points O′ and R′ divide the diagonal $M_3M_5$ of the bounding cell in the 1:1 ratio. (b) Projection of the patch onto the $x'y'$ plane showing the relationship between the $x'$ and $y'$ coordinates of the points O′, P′ and R′. (c) Projection of the patch onto the $z'x'$ plane showing the relationship between the $x'$ and $z'$ coordinates of the points O′, P′ and R′.

Twelve of these pieces combine to form a larger surface piece in the hierarchy of assembly, contained within a cube (Fig. 4a). We will refer to this cube of side a as the bounding cell of the G patch. The G surface is associate to both the D and P surfaces, being related by the Bonnet angle. The boundary of the patch of the D surface is defined by two straight lines (Fig. 2) which are embedded 2-fold axes, and one mirror plane curve. The converse is true for its adjoint twin, the P surface. However the boundary of the patch of the G surface is defined by neither straight lines nor mirror plane curves. Variation of the Bonnet angle produces a continuum of bent states intermediate between the D and P surfaces. The point-group symmetries assigned to the vertices are preserved. However, the G surface is unique in that these symmetry elements lock into the crystallographic space group $Ia\bar{3}d$. All other patches drawn from this continuum of states would produce surfaces with self-intersections if continued by these symmetry elements. Apart from the CLP surface and its homeomorphic adjoint, which are identical other than having different tetragonal proportions, the P, D and G surfaces are the only other example of intersection-free associate TPMS. It is considered highly unlikely that any other intersection-free TPMS containing neither straight lines nor plane lines of curvature are to be found. The effect of the Bonnet transformation is to transform the lattice of catenoidal channels into helicoidal strips, through a screw operation on the whole surface. The channels in both the P and D surfaces are transformed into spiral tunnels in the gyroid. The P surface contains plane holes which are almost circular in cross-section. Schwarz showed that these have radius variations of only ca. 0.4% [29]. These holes correspond to the almost helical geodesics on the G surface which have radius variations with respect to cylindrical helices of only ca. 0.5%. The four-fold screw isometries collapse to a screw of zero pitch but finite hole diameter for P, and reach a limit of finite pitch but zero hole diameter for D. The images of these hole curves in P and G are straight lines in D. The transformation of the quasi-circular holes in P into straight line holes in D, via the intermediate quasi-helical holes of the type which appear in G, is illustrated by the example of the line segment which is shown extending from left to right along the central axis of the fundamental

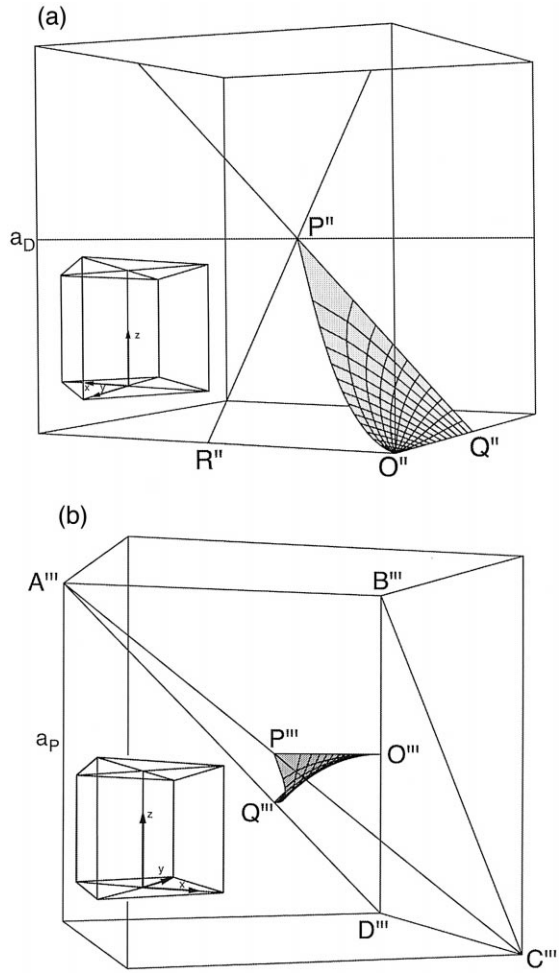


Fig. 2. (a) A patch of the D triply periodic minimal surface (associate to G) is bounded by the edges of the $O''P''Q''R''$ tetrahedron. The origin of the coordinate system imposed by the parametrization is at $O''$ and the orientation of the axes is shown in the inset. (b) A patch of the P triply periodic minimal surface (associate to G and conjugate to D) is bounded by the edges of the $O'''P'''Q'''R'''$ tetrahedron. The origin of the coordinate system imposed by the parametrization is at $O'''$ and the orientation of the axes is shown in the inset.

region of D. This line segment corresponds to a single pitch of the general quasi-helical hole curve. The diameter of such a quasi-helix is defined as the diameter of the closely similar circular helix which passes through the vertices of the regular map $\{6, 4|4\}$. Thus, the quasi-helix may be described as the circum-helix of the regular helical polygon, having a four-fold screw isometry which is a hole of the

regular map {6, 4|4} in the regular warped polyhedron which is homeomorphic to G. Due to its intermediate Bonnet angle with respect to the P and D surfaces, the G surface lacks straight lines (2-fold axes) and mirror planes. The volumes on either side of the gyroid surface are of symmetries $P4_132$ and $P4_332$, respectively. The volumes are therefore chiral, but in combination produce the symmetry $Ia\bar{3}d$, which is achiral. In its general morphology, G has a hybrid character with respect to P and D. The G surface has open round tunnels (in either labyrinth) which are centred on cube axes, or {1, 0, 0} directions, as does D. However, the tunnels in D are not straight, as they conform to the diamond-branched labyrinths of the surface. The G surface has a body centred cubic unit cell. Its primitive rhombohedral cell contains twelve G saddles and the cubic unit cell contains twenty-four. In this case the primitive rhombohedral cell is one half of the cubic unit cell. The integration domain is indicated by the shaded region in Fig. 3a.

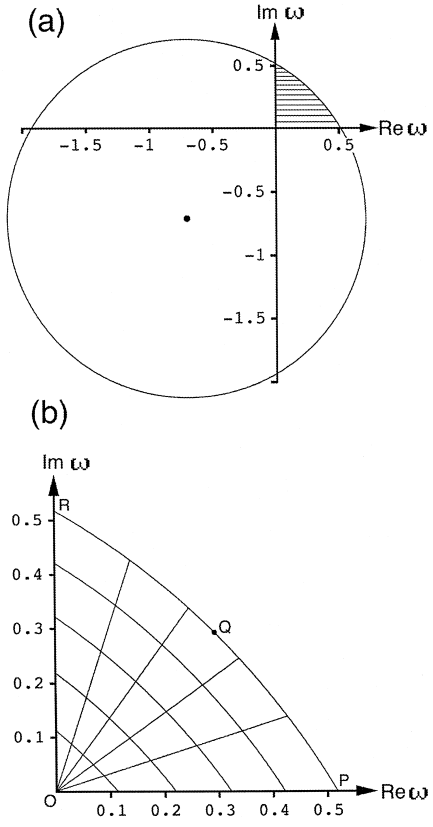


Fig. 3. (a) Integration domain of the G patch (shaded). (b) The $10\times10$ mesh used to compute the exact G surface. The complex plane coordinates of points O, P, Q and R are $O(0,0)$, $P((\sqrt{3}-1)/\sqrt{2},0)$, $Q((\sqrt{2}-1)/2,(\sqrt{2}-1)/2$ and $R(0,(\sqrt{3}-1)/\sqrt{2})$. The arc which bounds the domain is that of the circle of radius $\sqrt{2}$ centered at $(-\sqrt{2}/2,-\sqrt{2}/2)$.

## 3. Parametrization of the G surface

The Enneper–Weierstrass representation of the G surface involves integrals which can be evaluated analytically and are expressed in terms of the incomplete elliptic integral of the first kind, $F(\varphi, k^2)$. The modulus $k$ is real and lies in the interval [0, 1]. The amplitude $\varphi$ is a complex number. The complete elliptic integral of the first kind is a special case defined by the relation $K(k^2)=F(\pi/2, k^2)$. The properties of these two functions are described in standard texts on special functions [30–32]. Thus we give also a closed-form analytical expression for $\kappa$.

The Cartesian coordinates of any point on the G patch are obtained by combining (1) and (2) and setting $\theta_B = \mathrm{ArcCot}[K'/K]$, where $K = \mathrm{Elliptic}K[1/4]$, $K' = \mathrm{Elliptic}K[1/4]$ and $\omega_0 = 0$. The real space coordinates are given by

$$(x,y,z) = (\mathrm{Re}(x^*),\mathrm{Re}(y^*),\mathrm{Re}(z^*)) \tag{3a}$$

where

$$x^*(\omega) = I_0 - I_2$$

$$y^*(\omega) = \mathrm{i}(I_0 - I_2)$$

$$z^*(\omega) = 2I_1 \tag{3b}$$

and the $I_p$ are the integrals

$$I_p(\omega) = I_p(0) + \kappa\int_0^{\omega} \frac{\tau^p \mathrm{d}\tau}{\sqrt{\tau^8 - 14\tau^4 + 1}} \text{ with } p = 0, 1 \text{ and } 2. \tag{3c}$$

The variable limit $\omega$ is any complex point either inside or on the boundary of the domain shown in Fig. 3. With the double substitution $\tau = t^{1/2}$ and $s = t + 1/t$, the integrals (3c) are reduced to elliptic integrals [23]. These are expressed in terms of the

Legendre–Jacobi integrals to give the surface coordinates as

$$x = \kappa e^{i\theta}\,\mathrm{Re}\left\{\frac{1}{2\sqrt{2}}\,\mathrm{Elliptic}F \times\left[\mathrm{ArcSin}\left(\frac{2\sqrt{2}\,\omega}{\sqrt{\omega^4+4\omega^2+1}}\right),\frac{1}{4}\right]\right\}, \tag{4a}$$

$$y = \kappa e^{i\theta}\,\mathrm{Im}\left\{\frac{1}{2\sqrt{2}}\,\mathrm{Elliptic}F \times\left[\mathrm{ArcSin}\left(\frac{-2\sqrt{2}\,\omega}{\sqrt{\omega^4+4\omega^2+1}}\right),\frac{3}{4}\right]\right\}, \tag{4b}$$

$$z = \kappa e^{i\theta}\,\mathrm{Re}\left\{\frac{1}{4}\,\mathrm{Elliptic}F \times\left[\mathrm{ArcSin}\left(\frac{4\omega^2}{\omega^4+1}\right),97-56\sqrt{3}\right]\right\}, \tag{4c}$$

where $\theta = \mathrm{ArcCot}[K'/K]$.

The point $\omega = (\sqrt{3}-1)/\sqrt{2}$ (point Q in Fig. 2(b)) is a singular point of the Weierstrass function (2). However, in view of (3) the values of $x$(Q), $y$(Q) and $z$(Q) exist and are finite. The point $\omega = 0$ is mapped into (0, 0, 0). The coordinate frame is therefore defined jointly by the Weierstrass function (2) and the parametrization (Fig. 1a).

A closed-form analytical expression for $\kappa$ may be derived. The complex-plane coordinate of the point Q is $((\sqrt{3}-1)/\sqrt{2},0)$. When $\omega = (\sqrt{3}-1)/\sqrt{2}$, $\omega^2 = 2-\sqrt{3}$ and $\omega^2 = 7-4\sqrt{3}$. Substituting for $\omega$(Q) in (4) yields the image point of Q in $\mathscr{R}^3$

$$x(\mathrm{Q}) = aKK'/\sqrt{K''}\sqrt{2}$$

$$y(\mathrm{Q}) = -aKK'/\sqrt{K''}\sqrt{2}$$

$$z(\mathrm{Q}) = aKK'/2\sqrt{K''} \tag{5}$$

where $K'' = K^2 + K'^2$. The normalization constant

$$\kappa = a\sqrt{K''}/KK' \tag{6}$$

is thus strictly positive and its value is directly proportional to the edge length of the bounding cell. Substitution of (6) into (4) gives the full parametric equations for the G patch.

## 4. Properties of the G surface

The above results can be used to evaluate a number of geometrical properties of the G surface. For example, using (4) and (6) we verify that $z$(Q) $= -z$(R) $= a/2$.

The singular points of the Weierstrass function (2), O, P and R are mapped into the points O′(0, 0, 0), P′$(a/\sqrt{2}, -a/\sqrt{2}, a/2)$ and R′$(-a/\sqrt{2}, -a/\sqrt{2}, -a/2)$ on the G surface. Geometry dictates that the points P′ and R′ divide the cube edge $a$ in the ratio 1: 1 (Fig. 1(b)). The lengths O′P′, O′R′ and P′R′ are all invariants of the surface with values $a\sqrt{5}/2$, $a\sqrt{5}/2$ and $a\sqrt{3}$, respectively. There is no simple algebraic expression for the coordinates of the singular point Q. The points Q and R are related by symmetry, and although it is easily shown that P′Q′ = R′Q′, there seems to be no simple analytical expression for this length.

By setting $\beta = 0$ in (1) we obtain the patch of the D surface, associate to the G patch. The corresponding image points O″ and P″ have the coordinates O″(0, 0, 0), P″$(a/\sqrt{K''}/2\sqrt{2}K', 0, a\sqrt{K''}/4K')$. Similarly, setting $\beta = \pi/2$ we obtain the patch of the P surface, associate to the G patch. The corresponding image points O‴ and P‴ have the coordinates O‴(0, 0, 0), P‴$(0, -a\sqrt{K''}/2\sqrt{2}K, 0)$. The length O‴P‴ bisects the body diagonal of the cube of side $a_\mathrm{D}$ in one-half (see Fig. 2), and the length O‴P‴ cuts the face diagonal of the cube of side $a_\mathrm{P}$ in the same ratio. We therefore find that

$$a_\mathrm{D} = a\sqrt{K''}/2K' \tag{7}$$

$$a_\mathrm{P} = a\sqrt{K''}2K \tag{8}$$

These relationships enable us to derive exact analytical formulae for the perimeter $\mathscr{P}$, the surface area $\mathscr{A}$ and the normalized surface-to-volume ratio $\mathscr{A}/\mathscr{V}^{2/3}$ (since the ratio must be dimensionless we take $\mathscr{V}^{2/3}$ instead of $\mathscr{V}$) of the G patch.

The Bonnet transformation preserves the metric, the area and perimeter of all associate patches. The

Table 1
Cartesian coordinates $x'$, $y'$ and $z'$ of the twelve fundamental patches which make up the bounding cell of the G surface. The coordinates $x$, $y$ and $z$ are given by Eqs. (5) and (7). To compute the coordinates in the new frame, $\xi = 1/\sqrt{2}$ and $\eta = a/4$

| Patch | $x'$ | $y'$ | $z'$ |
|---|---|---|---|
| $P_1$ | $-\zeta x-\zeta y$ | $-\zeta x+\zeta y+2\eta$ | $z+3\eta$ |
| $P_2$ | $\zeta x-\zeta y$ | $-\zeta x-\zeta y+2\eta$ | $-z+3\eta$ |
| $P_3$ | $-\zeta x+\zeta y+2\eta$ | $z+3\eta$ | $\zeta x+\zeta y+4\eta$ |
| $P_4$ | $-\zeta x-\zeta y+2\eta$ | $-z+3\eta$ | $-\zeta x+\zeta y+4\eta$ |
| $P_5$ | $z+3\eta$ | $\zeta x+\zeta y+4\eta$ | $\zeta x-\zeta y+2\eta$ |
| $P_6$ | $-z+3\eta$ | $-\zeta x+\zeta y+4\eta$ | $\zeta x+\zeta y+2\eta$ |
| $P_7$ | $\zeta x+\zeta y+4\eta$ | $\zeta x-\zeta y+2\eta$ | $-z+\eta$ |
| $P_8$ | $-\zeta x+\zeta y+4\eta$ | $\zeta x+\zeta y+2\eta$ | $z+\eta$ |
| $P_9$ | $\zeta x-\zeta y+2\eta$ | $-z+\eta$ | $-\zeta x-\zeta y$ |
| $P_{10}$ | $\zeta x+\zeta y+2\eta$ | $z+\eta$ | $\zeta x-\zeta y$ |
| $P_{11}$ | $-z+\eta$ | $-\zeta x-\zeta y$ | $-\zeta x+\zeta y+2\eta$ |
| $P_{12}$ | $z+\eta$ | $\zeta x-\zeta y$ | $-\zeta x-\zeta y+2\eta$ |

patch perimeter $\mathscr{P}$ can therefore be simply evaluated from the associate D surface, since this patch is bounded by straight lines which the surface embeds. From Fig. 2 and using relationship (7) we deduce that

$$\mathscr{P} = a_D(\sqrt{2}-1) = a\sqrt{K''}/2K'. \quad (9)$$

If the area of the minimal surface bounded by a tetrahedron is $\mathscr{A}$, **r** is the inradius of a sphere which touches each face of that tetrahedron at one point (the inradius of the tetrahedron) and the length of the perimeter is $\mathscr{P}$, then [33]

$$\mathscr{A} = \mathscr{P}r/2. \quad (10)$$

The Coxeter cell of the P patch is the tetragonal disphenoid with inradius $\boldsymbol{r} = \boldsymbol{a}_P(\sqrt{2}-1)/2$. By substituting (8) and (9) into (10), we see that $\mathscr{A} = a^2K''/8KK'$. The volume of the quadrirectangular tetrahedron enclosing the G patch is $a^3/3$, so

$$\mathscr{A}/\mathscr{V}^{2/3} = (3^{2/3}/8)K''/KK' = 0.535871853\ldots$$
(for the fundamental patch)

$$\mathscr{A}/\mathscr{V}^{2/3} = (3/32^{1/2})K''/KK' = 1.947487558\ldots$$
(for the primitive rhombodral cell)

$$\mathscr{A}/\mathscr{V}^{2/3} = (3/4^{2/3})K''/KK' = 2.453680569\ldots \text{ (for the bcc unit cell)}.$$

## 5. Computation of the G surface

Schoen's paper which describes the G surface for the first time shows only photographs of plastic models of the surface (Fig. 7 in Ref. [6]). An exact

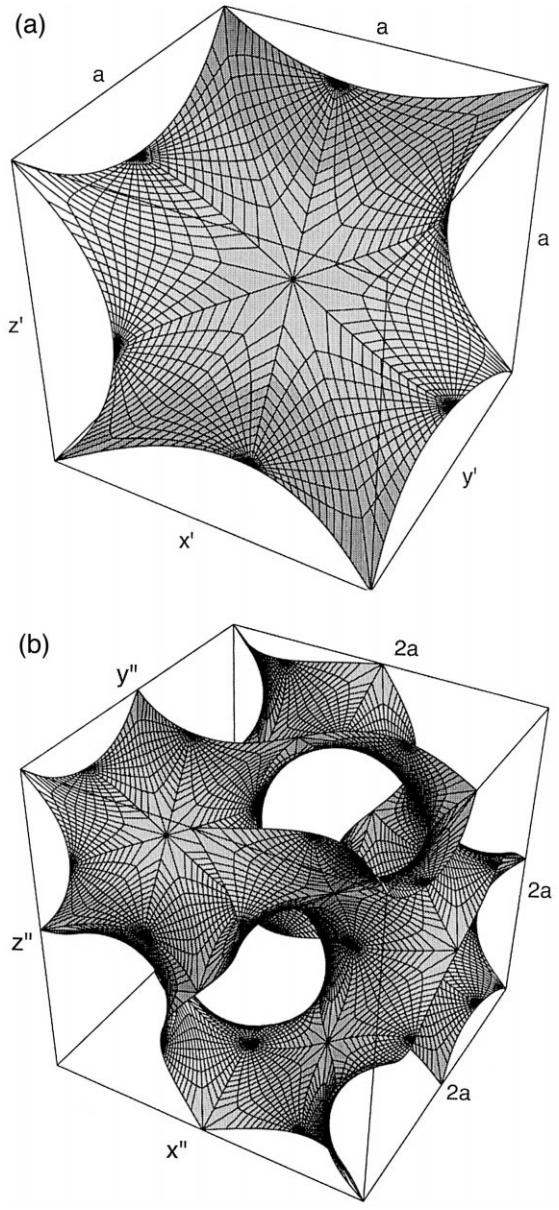


Fig. 4. (a) A piece of the G surface composed of 12 fundamental patches is inscribed in the bounding cell. (b) The face-centred cubic unit cell of the G surface made by combining the eight pieces shown in (a).

Table 2
Cartesian coordinates $x''$, $y''$ and $z''$ of the eight bounding cells which comprise the face centred cubic unit cell of the G surface. The coordinates $x'$, $y'$ and $z'$ are given in Table 1 and $\eta = a$

| GCellOctant | x″ | y″ | z″ |
|---|---|---|---|
| $O_1$ | $x'$ | $y'$ | $z'$ |
| $O_2$ | $-x'+2\eta$ | $-y'+\eta$ | $z'$ |
| $O_3$ | $-x'+\eta$ | $y'+\eta$ | $z'$ |
| $O_4$ | $x'+\eta$ | $-y'+2\eta$ | $z'$ |
| $O_5$ | $x'$ | $-y'+\eta$ | $z'-\eta$ |
| $Q_6$ | $-x'+2\eta$ | $y'$ | $z'-\eta$ |
| $Q_7$ | $-x'+\eta$ | $-y'+2\eta$ | $z'-\eta$ |
| $O_8$ | $x'+\eta$ | $y'+\eta$ | $z'-\eta$ |

computation of the surface is as follows. The evaluation of the elliptic functions given above is fast and straightforward. The Mathematica computer program (Wolfram Research) has elliptic functions built in as user-callable subroutines.

The Cartesian coordinates of the points of the G patch were computed using (4) and (6) using a $10 \times 10$ mesh (Fig. 3b). Larger surface pieces are conveniently calculated by transforming the coordinate system to that of Fig. 1a by a rotation of $-\pi/4$ about the $z$ axis, reflecting in the $yz$ plane and translating the origin along the vector $(0, 1/2, 3/4)$. The effect is the creation of a new coordinate frame with origin at $M_1$ whose edges $M_1M_2$, $M_1M_4$ and $M_1M_5$ determine the $x'$, $y'$ and $z'$ axes, respectively (Fig. 1). The new coordinates of the G patch are those of $P_1$ (Table 1).

While the G surface embeds only an inversion centre, the bounding cell of the G patch is composed of twelve congruent parts related by 2-fold rotational axes and mirror planes. There are two types of diad axes: four passing through the corners of the bounding cell and the inversion centre, and six which bisect six of the twelve edges of the bounding cell and define a skew straight-edged hexagon which encloses the twelve patches of the cell (Fig. 4a). The bounding cell represents the second order of hierarchy for the construction of the fcc unit cell of the G surface. Thus it is used as the fundamental building block in the next stage of construction. The eleven remaining patches $F_i$ ($i = 2$–12) were generated from $F_1$ by the successive symmetry operations summarised in Table 1. $F_1$ generates $F_2$ and so on pairwise.

Eight bounding cells combine using the symmetry operations summarised in Table 2, to give the full face centred cubic unit cell of the G surface. The last four are related to the first four by a mirror plane which passes through the centre of the cell parallel to its top and bottom face and which divides it into two equal half volumes (Fig. 4b).

## 6. Conclusions

Integration of the Enneper–Weierstrass representation of the G minimal surface with the Weierstrass function of the form $R(\tau) = (1)/\sqrt{\tau^8 - 14\tau^4 + 1}$ and the Bonnet angle of $\theta = 38.0147°$ (with respect to the D surface) enabled us to obtain analytical expressions for the Cartesian coordinates of the fundamental patch of the surface. The surface-to-volume ratio of the fundamental patch is 0.535871853.... Symmetry considerations allowed us to construct a piece of the surface composed of 12 fundamental patches, and finally the face-centred cubic unit cell of the surface composed of 96 fundamental patches.

## References

[1] M.P. do Carmo, Differential Geometry of Curves and Surfaces, Prentice-Hall, Engelwood Cliffs, NJ, 1976.
[2] S. Hyde, S. Andersson, K. Larsson, Z. Blum, T. Landh, S. Lidin, B.W. Ninham, The Language of Shape. The Role of Curvature in Condensed Matter: Physics, Chemistry and Biology, Elsevier, Amsterdam, 1997.
[3] H.U. Nissen, Science 166 (1969) 1150.
[4] F.J. Almgren, The Mathematical Intelligencer 4 (1982) 164.
[5] M. Kemp, Nature 389 (1997) 919.
[6] A.H. Schoen, Infinite Periodic Minimal Surfaces Without Self-Intersections, NASA Technical Note D-5541, NASA, 1970.
[7] S. Förster, A.K. Khandpur, J. Zhao, F.S. Bates, I.W. Hamley, A.J. Ryan, W. Bras, Macromolecules 27 (1994) 6922.
[8] V. Luzzati, P.A. Spegt, Nature 215 (1967) 701.
[9] H.G. von Schnering, R. Nesper, Angew. Chem. Int. Ed. Engl. 26 (1987) 1059.
[10] H.G. von Schnering, R. Nesper, Z. Phys. B 83 (1991) 407.
[11] R.T. Blunt, J. Phys. E 13 (1980) 1149.
[12] T. Landh, Federation of European Biochemical Societies (FEBS) Letters 369 (1995) 13.
[13] C.T. Kresge, M.E. Leonowicz, W.J. Roth, J.C. Vartuli, J.S. Beck, Nature 359 (1992) 710.

[14] D.M. Anderson, P. Ström, Physica A 176 (1991) 151.
[15] V. Alfredsson, M.W. Anderson, T. Ohsuna, O. Terasaki, M. Jacob, M. Bojrup, Chem. Mater. 9 (1997) 2066.
[16] M.W. Anderson, Zeolites 19 (1997) 220.
[17] A. Baiker, Current Opinion in Solid State and Materials Science 3 (1998) 86.
[18] W.T.A. Harrison, T.E. Gier, G.D. Stucky, R.W. Broach, R.A. Bedard, Chem. Mater. 8 (1996) 145.
[19] A. Katz, M.E. Davis, Nature 403 (2000) 286.
[20] J.C.C. Nitsche, Lectures on Minimal Surfaces, Vol. 1, Cambridge University Press, Cambridge, 1989.
[21] D. Cvijović, J. Klinowski, J. Phys. (Paris) I 2 (1992) 2207.
[22] D. Cvijović, J. Klinowski, J. Phys. (Paris) I 2 (1992) 2191.
[23] D. Cvijović, J. Klinowski, J. Phys. (Paris) I 2 (1992) 137.
[24] D. Cvijović, J. Klinowski, J. Phys. (Paris) I 3 (1993) 909.
[25] D. Cvijović, J. Klinowski, Chem. Phys. Lett. 226 (1994) 93.
[26] P.J.F. Gandy, D. Cvijović, A.L. Mackay, J. Klinowski, Chem. Phys. Lett. 314 (1999) 543.
[27] A. Fogden, S.T. Hyde, Acta Crystallogr. A 48 (1992) 575.
[28] H.S.M. Coxeter, Regular Polytopes, 2nd ed., Macmillan, New York, 1963.
[29] H.A. Schwarz, Gesammelte Mathematische Abhandlungen, Springer, Berlin, 1890.
[30] M. Abramowitz, I.A. Stegun, Handbook of Mathematical Functions, Dover, New York, 1980.
[31] I.S. Gradshteyn, I.M. Ryzhik, Tables of Integrals, Series and Products, Academic Press, New York, 1980.
[32] J. Spanier, K.B. Oldham, An Atlas of Functions, Springer-Verlag, Berlin, 1987.
[33] B. Smyth, Inventiones Mathematicae 76 (1984) 411.